Secondary-Electron-Emission Instability in a Plasma

M. C. Griskey* and R. L. Stenzel

Department of Physics and Astronomy, University of California, Los Angeles, California 90095-154705

(Received 29 June 1998)

A 200-eV electron beam is incident on an electrode in a laboratory plasma. The emission of secondary electrons produces a region of negative differential resistance in the current-voltage characteristic of the electrode. Spontaneous dynatron oscillations are driven by the negative differential resistance when a resonant circuit is placed in series with the electrode. The instability is driven by the beam energy, produces large amplitudes comparable to the beam voltage, modulates beam and plasma parameters, and excites plasma eigenmodes such as ion acoustic waves. [S0031-9007(98)08228-3]

PACS numbers: 52.40.Hf, 52.35.Qz, 52.40.Fd, 52.70.Ds

The interaction of electron beams with plasmas has been studied extensively. For example, in space plasmas attention has been focused on natural electron beams in the aurora [1] and artificially injected beams from spacecraft [2], in the laboratory electron beams are used in dc discharges [3], turbulent heating of fusion plasmas [4], generation of coherent radiation sources [5], and laser-based particle accelerators [6]. Numerous instabilities can be excited by beams in resonance with waves. These may be supported by slow wave structures in free space [7], plasma eigenmodes such as Langmuir waves [8], or oblique whistler waves [9]. When the electron beam interacts with boundaries, secondary electron emission occurs [10], which can produce a different class of instabilities. These are based on the negative differential resistance of the current-voltage, I-V, characteristic of the collecting-emitting electrode. Such dynatron oscillations have been studied in vacuum tubes [11] but, to our knowledge, not in plasmas. Of course, the dc characteristic of Langmuir probes subject to secondary electron emission are well known [12,13]. In this Letter, we report experimental observations of the secondary-electron-emission instability in an unmagnetized discharge plasma. The salient features of the instability are as follows: (i) large-amplitude oscillations bounded by the plasma potential and the beam potential; (ii) frequencies determined by the circuit inductance and the sheath capacitance; (iii) the beam providing the free energy for the instability which can operate at zero dc current to the electrode; (iv) that the instability can arise between two floating electrodes connected by an inductor, one of which is emitting secondary electrons; (v) that the instability excites plasma eigenmodes, e.g., ion acoustic waves or Langmuir wave sidebands. The instability is not only of intrinsic interest in basic plasma physics but may arise on long spacecraft structures bombarded by energetic electrons [14] of Langmuir probes terminated by inductors in electron beams [15] where the oscillations might be mistaken as a beam-plasma instability.

The experiments, performed as part of a university course in experimental plasma physics [16], are conducted in a 1.2 m long, 40 cm diameter cylindrical plasma device shown in Fig. 1. A discharge plasma ($n_e \approx 10^9$ cm^{-3}, $kT_e \approx 3$ eV, $p_n = 3 \times 10^{-4}$ Torr Ar) is created by an electron beam ($V_b = 100$–300 V, $I_b = 20$–500 mA) emitted from 2.5-cm-diameter oxide-coated cathode. The plasma density is independently obtained from Langmuir probe traces and an rf probe measuring the electron plasma frequency ($\omega_{pe}^2 = n_e e^2/m_e \varepsilon_0$), while the electron temperature is found from both Langmuir probes and the speed of ion acoustic waves ($c_s^2 = kT_e/m_i$).

Various electrodes are placed in different locations both within and outside of the beam. These include plane wire grids (stainless steel, 3×3 cm^2 and 7.5×7.5 cm^2, 50% transparent) and a plane Langmuir probe (3.7-mm diameter Ta). Depending on the measurements performed, different electrical circuits are attached to the electrodes. The dc I-V characteristics are obtained by biasing the electrodes with respect to the grounded chamber wall. To produce ac oscillations, a resonant circuit is connected in series with the dc bias supply whose internal impedance is negligible. Oscillations are generated with either grids or Langmuir probes connected to ground or interconnected as double electrodes which float electrically with respect to ground.

The experimental results start with a brief review of the dc I-V characteristics of an electrode in a beam-plasma system. Figure 2 shows a plot of $-I_{\text{grid}}$ vs V_{grid} with a 197-eV beam normal to the grid. For grid

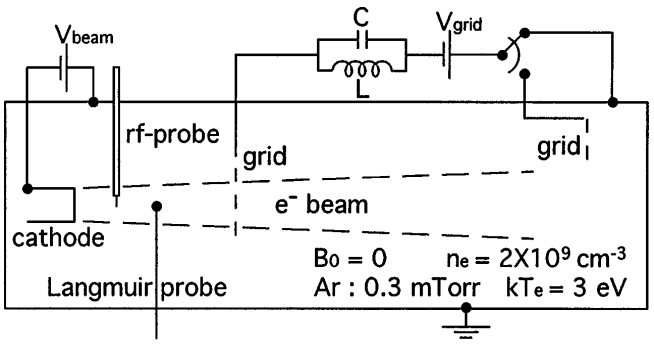

FIG. 1. Experimental setup.

 0031-9007/99/82(3)/556(4)$15.00

voltages more negative than the beam voltage, only the ion saturation current is collected. As the grid voltage is increased, the grid collects beam electrons. When the currents due to ions and beam electrons balance, the grid is at its first floating potential, $V_{f,1}$. For grid voltages more positive than $V_{f,1}$, the current is first dominated by the flux of beam electrons, but then reduced due to the emission of secondary electrons. Note that the emission of secondaries produces a positive current, while the collection of beam electrons results in a negative current. When the beam electron current is balanced by both the secondary electron current and the ion current, the grid is at its second floating potential, $V_{f,2}$. Note that the I-V characteristics have a negative differential resistance, $(\partial I/\partial V)^{-1} < 0$, hence $V_{f,2}$ is an unstable floating potential. The negative resistance arises from the fact that, as the voltage on the grid is increased, the beam electrons strike the grid with a higher energy and create a higher emission current of secondary electrons, which reduces the net current. When the grid voltage is further raised, the thermal electrons of the discharge plasma are collected. When the currents of the plasma electrons, beam electrons, secondary electrons, and ions all balance, the grid is at its third floating potential, $V_{f,3}$. For grid voltages larger than $V_{f,3}$, the plasma electron current would exponentially grow and saturate at the plasma potential as with the standard Langmuir I-V trace.

Spontaneous voltage oscillations are generated in a parallel LC resonant circuit connected in series with electrodes biased in the negative resistance range. The oscillation frequency depends on the external circuit elements as well as the plasma parameters via the sheath capacitance. Typical values range from 10 kHz to 10 MHz, compared to typical plasma frequencies of ions, $f_{pi} = 1.5$ MHz, and electrons, $f_{pe} = 400$ MHz. The highest frequency, obtained without external capacitance, is determined by the sheath capacitance. Because of sheath expansion, the frequency increases with dc bias voltage and decreases with plasma density. The oscillation amplitude depends on the circuit losses, i.e., equivalent parallel resistance, compared to the negative differential resistance which depends on amplitude. For larger beam currents, the negative differential resistance is smaller; hence, for given circuit losses, the instability amplitude increases until they are clipped. The oscillations are clipped by the steep rise of the I-V curve near the plasma potential and, to a lesser degree, by the positive differential resistance near $V_{f,1}$. There is also a slight negative frequency shift for increasing oscillation amplitude ($\Delta f/\Delta V \approx -0.5$ kHz/V) at a constant dc bias.

Plots of the voltage and current oscillations are shown in Fig. 3 which shows the voltage and current oscillations on a wire grid connected to ground via a parallel LC circuit, $L = 5.3$ mH and $C = 23$ pF (partly due to the capacitive coupling between the grid and the plasma) and a voltage bias. Figure 3 shows the voltage on the grid while it is swept from -220 V to 7 V and being exposed to a 197 V, 100 mA electron beam. As the voltage sweeps though the negative resistance region, voltage oscillations, with a frequency given by $\frac{1}{2}\pi\sqrt{LC} = 455$ kHz, appear on the grid. Figure 3(b)

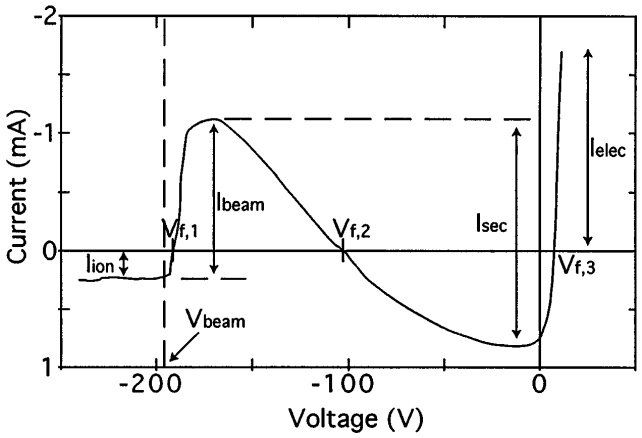

FIG. 2. dc current-voltage characteristic of a grid in an electron beam subject to secondary electron emission.

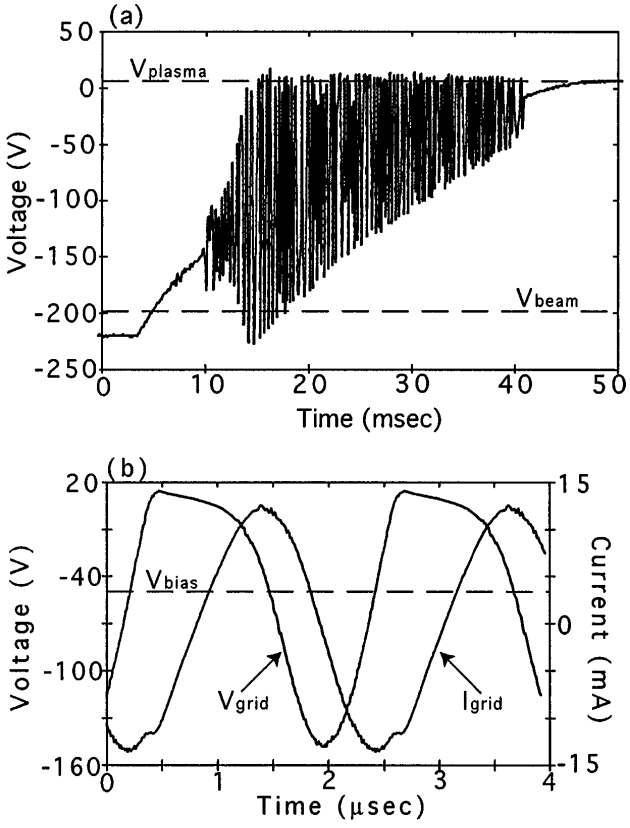

FIG. 3. (a) Voltage sweep of a wire grid exposed to an electron beam shown as a function of time. Spontaneous voltage oscillations appear over the negative differential resistance region of the wire grid and are clipped at the plasma potential, $V_{\text{plasma}} = 7$ V. (b) A detailed plot of the voltage vs time and current vs time oscillations. The grid bias, $V_{\text{bias}} = -50$ V, is shown as a dashed line.

shows an expanded view of Fig. 3(a) at a fixed grid voltage $V_{\text{bias}} = -50$ V. The voltage oscillates around the dc bias and is clipped just above the plasma potential $V_{plasma} = 7$ V. Fourier analysis reveals a spectrum with many harmonics of the fundamental instability. These could produce electromagnetic radiation for frequencies larger than the electron plasma frequency.

These grid oscillations modulate the electron beam current, causing slight charge imbalances. This creates an oscillating electric field at the beam edge which launches ion acoustic waves that propagate radially outward from the beam. Figure 4 shows the results of interferometry measurements taken between grid oscillations and fluctuations in the electron saturation current ($J_{\text{sat}} \approx -en\sqrt{2kT_e/m_e}$) measured by a movable Langmuir probe. Figure 4(a) shows the dispersion relation generated by measuring the wavelength corresponding to several grid instability frequencies. The straight line fit to the data yields a sound speed of 2.5×10^5 cm/s which is in good agreement with the value calculated from Langmuir probe temperature measurements, 2.7×10^5 cm/s. Figure 4(b) presents a 2-dimensional plot that shows lines of density maxima and minima (phase fronts) of 200 kHz ion acoustic waves. The plot clearly shows propagation radially outward from the electron beam. The apparent increase in wavelength at distances far from the beam is a result of the curved path taken by the Langmuir probe.

In addition to launching ion acoustic waves, the secondary emission grid instability creates sidebands in the beam-plasma instability resonance curve. Figure 5 shows the spectrum analysis of rf probe data taken 17 cm from the primary beam source with a 3×3 cm^2 grid in between. Figure 5(a) was taken with zero bias, and hence no oscillations, on the grid. A resonance peak is seen just above the plasma frequency that arises due to the beam-plasma instability ($\nu_{\text{beam}} \approx \omega_{pe}/k_{\text{Landau}}$). When a -75 V bias is placed on the grid, causing 8.6 MHz oscillations due to the secondary emission instability, the spectrum appears as in Fig. 5(b). Sidebands form near the beam-plasma instability resonance at the frequency of the secondary emission instability above and below the plasma frequency, $f_{pe} \pm f_{\text{inst}}$. These sidebands form because of the density modulation of the electron beam by the voltage oscillations on the grid. Note that the plasma frequency f_{pe} is slightly reduced in Fig. 5(b) corresponding to a 2% reduction in the plasma density n_e. This is caused by the negative bias on the grid which lowers the plasma potential, the primary electron beam current, and thereby the density.

The present set of experiments has shown how electrodes exposed to electron beams can exhibit a secondary electron emission instability. In an unmagnetized plasma, the instability was shown to be able to couple to the ion acoustic mode and to modulate the frequency of the beam-plasma instability. In a magnetized plasma, the secondary electron emission instability could couple to the whistler mode and the Alfvén mode.

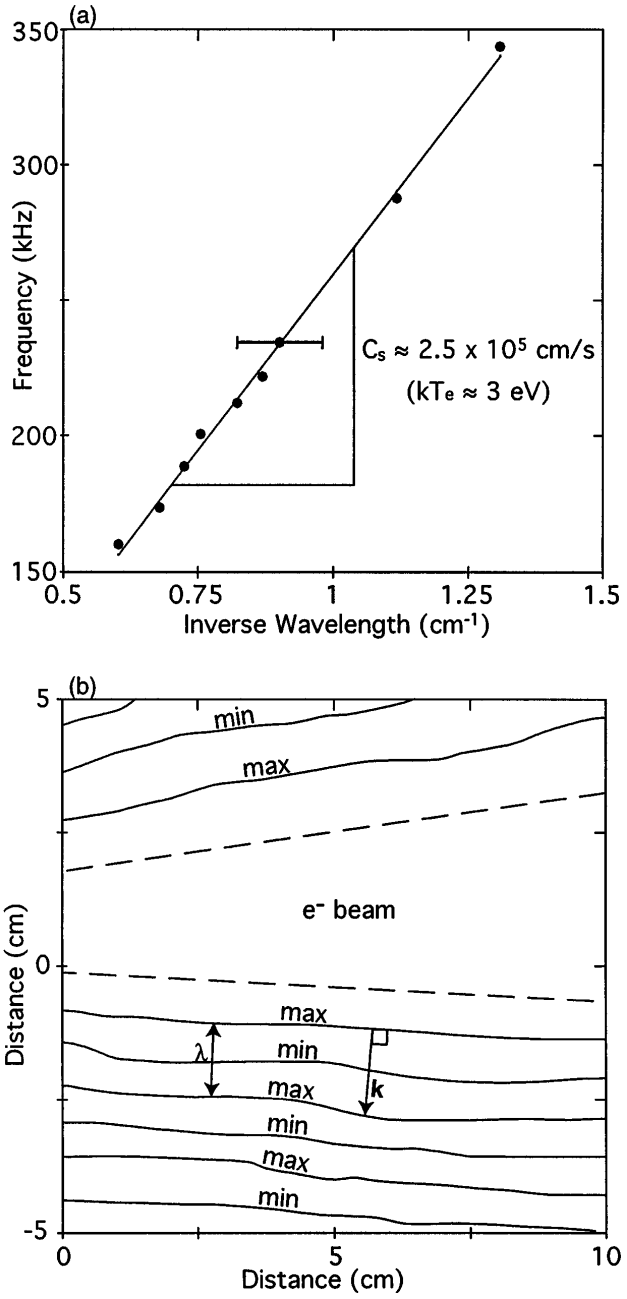

FIG. 4. Interferometry measurements of ion acoustic waves. (a) Dispersion relation for ion acoustic waves yielding a sound speed of 2.5×10^5 cm/s. (b) Phase fronts of 200 kHz ion acoustic waves measured with inteferometry techniques which show propagation perpendicular to the beam.

The secondary electron emission instability can occur when the following conditions are met: First, two electrodes must be present in the plasma with at least one being bombarded by primary electrons; second, the electrodes must be inductively coupled (the capacitive coupling between the electrode and the plasma was enough

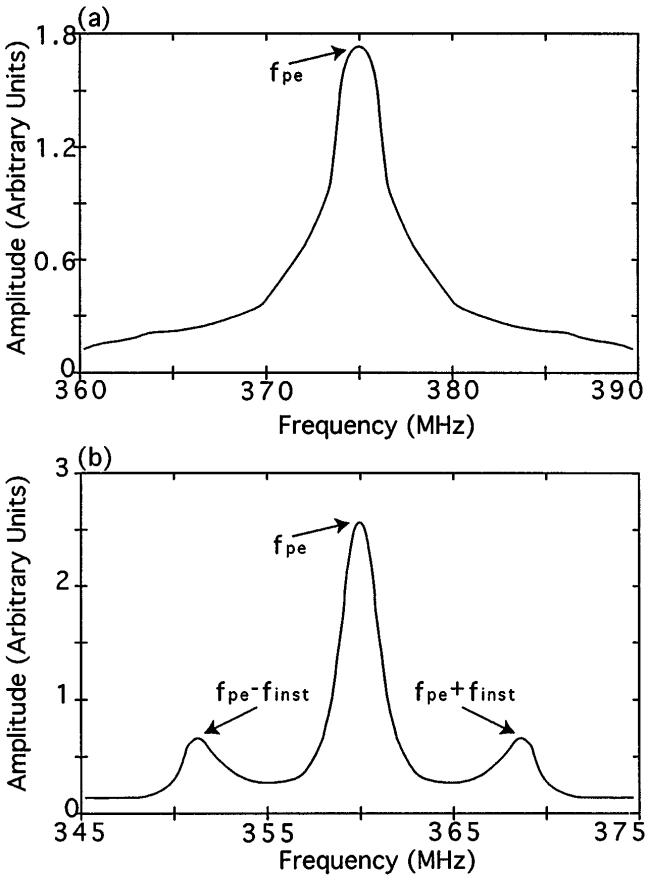

FIG. 5. rf probe measurements showing the beam-plasma instability. (a) The beam plasma instability in the absence of the secondary emission instability showing a resonance just above the electron plasma frequency, $f_{pe} = 375$ MHz. (b) The beam plasma instability in the presence of the secondary electron emission instability showing sidebands at the secondary emission instability frequency above and below the plasma frequency, $f_{pe} \pm f_{\text{inst}}$. The plasma frequency is lower in this case because of the large bias on the grid as explained in the text.

for the highest frequency oscillations); third, the electrode being bombarded by the primary electrons must be initially forced to a potential more negative than the other electrode (by about half the beam energy in volts). The last condition need not be met by using an external power supply (as was done in this set of experiments). An extended conducting structure moving through a magnetic field could become sufficiently charged to induce these oscillations. Note also that a large conducting structure can have a high self-inductance. In light of this, it is possible for extended satellite-tether systems moving through a magnetic field and being exposed to an electron beam to exhibit the oscillations presented here. It would be easy to mistake these oscillations or the effects of these oscillations on the surrounding plasma for naturally occurring plasma instabilities. Plasma studies that use inductance to filter out high frequency signals received by Langmuir probes in the presence of electron beams could also produce this instability.

*Electronic address: griskey@physics.ucla.edu

[1] S.-I. Akasofu, *Physics of Auroral Arc Formation, Proceedings of the Chapman Conference*, edited by S.-I. Akasofu and J. R. Kan (Am. Geophys. Union, Washington, DC, 1981), Vol. 26, pp. 1–14.
[2] T. Neubert and P. M. Banks, Planet. Space Sci. **40**, 153 (1992).
[3] I. Langmuir, J. Appl. Phys. **19**, 231 (1925).
[4] A. A. Rukhadze, K. A. Sarksyan, and N. N. Skvortsova, J. Phys. IV (France) (C6) **5**, 53 (1995).
[5] S. H. Gold and G. S. Nusinovich, Rev. Sci. Instrum. **68**, 3945 (1997).
[6] C. E. Clayton *et al.*, Phys. Plasmas **1**, 1753 (1994).
[7] J. R. Pierce, *Travelling-Wave Tubes* (D. Van Nostrand Co., Inc., New York, 1950).
[8] R. J. Briggs, *Electron-Stream Interactions with Plasmas* (MIT Press, Cambridge, MA, 1964).
[9] R. L. Stenzel, J. Geophys. Res. **82**, 4805 (1977).
[10] R. Kollath, *Encyclopedia of Physics XXI*, edited by S. Fluegge (Springer, Berlin, 1956), pp. 232–291.
[11] A. W. Hull, Proc. Inst. Radio Electron. Eng. Aust. **6**, 5 (1918).
[12] K. Wiesemann, Ann. Phys. (Leipzig) **27**, 303 (1971).
[13] C. H. Nam *et al.*, J. Appl. Phys. **63**, 5674 (1988).
[14] N. H. Stone and C. Bonifazi, Geophys. Res. Lett. **25**, 409 (1998).
[15] H. Gunell and T. Löfgren, Phys. Plasmas **4**, 2805 (1997).
[16] http://www.physics.ucla.edu/plasma-exp/180E-W97